J Electr Eng Technol Vol. 8, No. 2: 304-315, 2013
http://dx.doi.org/10.5370/JEET.2013.8.2.304

ISSN(Print) 1975-0102
ISSN(Online) 2093-7423

Analysis of Cascaded H-Bridge Multilevel Inverter in DTC-SVM Induction Motor Drive for FCEV

Javad Gholinezhad† and Reza Noroozian*

Abstract – In this paper, analysis of cascaded H-bridge multilevel inverter in DTC-SVM (Direct Torque Control-Space Vector Modulation) based induction motor drive for FCEV (Fuel Cell Electric Vehicle) is presented. Cascaded H-bridge multilevel inverter uses multiple series units of H-bridge power cells to achieve medium-voltage operation and low harmonic distortion. In FCEV, a fuel cell stack is used as the major source of electric power moreover the battery and/or ultra-capacitor is used to assist the fuel cell. These sources are suitable for utilizing in cascaded H-bridge multilevel inverter. The drive control strategy is based on DTC-SVM technique. In this scheme, first, stator voltage vector is calculated and then realized by SVM method. Contribution of multilevel inverter to the DTC-SVM scheme is led to achieve high performance motor drive. Simulations are carried out in Matlab-Simulink. Five-level and nine-level inverters are applied in 3hp FCEV induction motor drive for analysis the multilevel inverter. Each H-bridge is implemented using one fuel cell and battery. Good dynamic control and low ripple in the torque and the flux as well as distortion decrease in voltage and current profiles, demonstrate the great performance of multilevel inverter in DTC-SVM induction motor drive for vehicle application.

Keywords: Cascaded H-bridge multilevel inverter, Space Vector Modulation (SVM), Direct Torque Control (DTC), Induction motor drive, Fuel Cell Electric Vehicle (FCEV).

1. Introduction

In recent years, industry has begun to demand higher power equipment, which now reaches the megawatt level [1]. The multilevel converter is a promising power electronics topology for high power motor drive applications because of its low electromagnetic interference (EMI) and high efficiency [1-4]. These inverters can solve the problems associated with traditional 2-level inverters. Their topologies, including diode-clamped, flying capacitor, and cascaded H-bridge structures, are intensively studied for high-power applications [1, 5, 6]. In cascaded H-bridge the desired output voltage is obtained by combining several separate DC voltage sources. Solar cells, fuel cells, batteries, and ultra-capacitor are the most common used independent sources [3]**.** This structure can be considered in two arrangements, symmetrical and asymmetrical. The use of asymmetric input voltages can reduce, or when properly chosen, eliminate redundant output levels. In addition more different output voltage levels can be generated with the same number of components, compared to a symmetric multilevel inverter [6-9]. Higher output quality can be obtained with fewer cascaded cells and control complexity, and output filters can be remarkably shrunk or even eliminated [6].

† Corresponding Author: Dept. of Electrical Engineering, University of Zanjan, Zanjan, Iran. (javad.gholinezhad@gmail.com)
* Dept. of Electrical Engineering, University of Zanjan, Zanjan, Iran. (noroozian@znu.ac.ir)
Received: February 3, 2012; Accepted: September 13, 2012

Direct Torque Control (DTC) is one of the most popular control strategies in high-performance variable-speed drive applications for induction machines, which it can decouple the interaction between flux and torque control, and provide good torque response in steady state and transient operation conditions [10]. Simple structure and very good dynamic behaviour are main features of DTC. However, classical DTC has several disadvantages, from which most important is variable switching frequency [11]. To eliminate the disadvantages of the classical DTC methods, Direct Torque Control-Space Vector Modulation (DTC-SVM) has been developed. Basically in DTC-SVM, the controllers calculate the required stator voltage vector and then it is realized by space vector modulation technique. With respect to the advantages of multilevel inverter and DTC-SVM method for good utilization in motor applications, using multilevel inverter in DTC-SVM induction motor drive, can lead to achieve high performance drive for motor applications.

Today's with the highly developed automotive industry and increase the number of automobiles in use around the world, the environment problems (air pollution and global warming issues) and depleting petroleum resources are becoming serious threats to modern life [12]. These problems indicate a safer, cleaner and more efficient vehicle than the conventional vehicle is needed. Fuel cell has several advantages include clean by-product, quiet operation and have high power density and high efficiency which make it suitable for vehicle application. FCEVs are

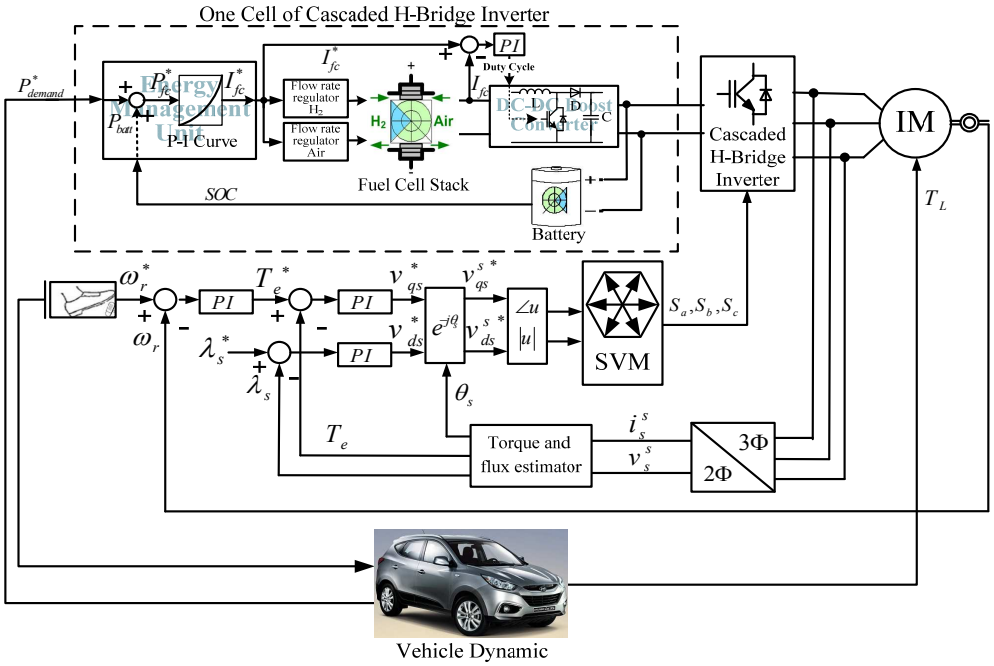

Fig. 1. The block diagram of DTC-SVM based induction motor drive for FCEV application by cascaded H-bridge inverter.

one of the most promising vehicle solutions for the foreseeable future [12]. In FCEV, a fuel cell stack is used as the major source of electric power moreover the battery and/or ultra-capacitor is used to assist the fuel cell stack.

For FCEV a cascaded H-bridge inverter can be used to drive the traction motor from a set of fuel cell or batteries [13]. Several authors have addressed the using of multilevel inverter in large electric drive application to meet the high power demands. In [2, 4, 13, 14] cascaded H-bridge multilevel inverter has been used by fundamental frequency switching scheme for decreasing the harmonic distortion in output voltage. Symmetrical and asymmetrical arrangements have been used in [6, 15] in DTC induction motor drive by modified lookup table to improve the torque and flux profile. This paper proposes application of cascaded H-bridge multilevel inverter in induction motor drive for FCEV by DTC-SVM technique to improve the torque and the flux behaviour as well as distortion decrease in voltage and current profiles. The SVM method can be used for both symmetrical and asymmetrical inverters. The motor reference power and torque are calculated in vehicle dynamic and the energy management units control the reference power of fuel cell stacks.Cell schematic layout of this paper is shown in Fig. 1. The reminder of the paper is organized as follows. Section 2 introduces cascaded H-bridge inverter. SVM in cascade H-bridge inverter and DTC-SVM have been presented in sections 3 and 4, respectively. Sections 5 and 6 describe vehicle dynamic model and FCEV power sources model and control, respectively. Simulation results have been provided in section 7. Finally section 8 concludes this paper.

2. Cascaded H-Bridge Inverter

Cascaded H-bridge multilevel inverter is one of the popular converter topologies used in high-power Medium-Voltage (MV) drives [16]. As the name suggests, the cascaded H-bridge multilevel inverter has been used multiple units of H-bridge power cells connected in a series to achieve medium-voltage operation and low harmonic distortion [17]. This inverter needs several DC voltage sources to synthesize output voltage waveform, which solar cells, fuel cells, batteries and ultra capacitor are the most common independent sources. The structure of this inverter is shown in Fig. 2, which each phases consist of two H-bridge. The single H-bridge is a three-level inverter that the four switches S_{i1}, S_{i2}, S_{i3} and S_{i4} can be controlled to generate three-level output, $\pm V_{dci}$ and 0, when S_{i1} and S_{i4} are on, the output is $+V_{dci}$; when S_{i2} and S_{i3} are on, the

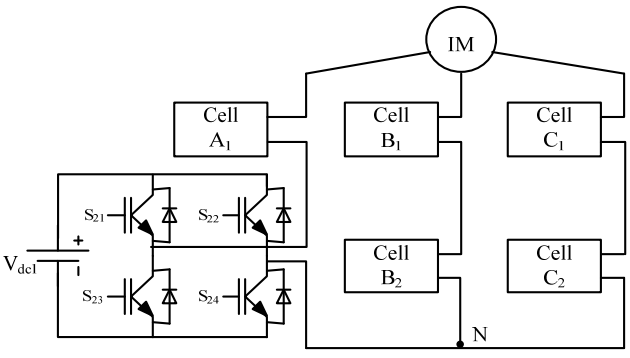

Fig. 2. Cascaded H-bridge multilevel inverter.

output is $-V_{dci}$; when either pair S_{i1} and S_{i2} or S_{i3} and S_{i4} are on, the output is 0.

In modular or symmetric structure of cascaded H-bridge inverter which the DC voltage sources are equal, there are $2N+1$ level in output of phase voltage where N is the number of DC voltage sources. Different levels of five-level are given in Table 1. P and N mean positive and negative outputs of H-bridge, respectively. The use of asymmetric input voltages (inverter fed by a set of DC voltage sources where at least one of them is different from the other one) can reduce, or when properly chosen, eliminate redundant output levels, maximizing the number of different levels generated by the inverter. Therefore, this topology can achieve the same output voltage quality with fewer numbers of semiconductors [6, 8]. The optimal asymmetry has been obtained using voltage sources proportionally scaled to the two- or three- H-bridge power that the number of levels in phase voltage obtains as follows:

$$\begin{aligned} &\text{if} \quad V_{dci} = 2^{(i-1)}E,\ i = 1,2,...,N \rightarrow n = 2^{(N+1)} - 1 \\ &\text{if} \quad V_{dci} = 3^{(i-1)}E,\ i = 1,2,...,N \rightarrow n = 3^{N} \end{aligned} \tag{1}$$

where, N is the number of DC voltage sources. For cascaded H-bridge inverter shown in Fig. 2 is generated seven-level and nine-level inverters by asymmetry structure that H-bridge scaled to the 2 and 3, respectively. Different levels of nine-level inverter are given in Table 2.

Table 1. Voltage Levels of Five-level Inverter

Output voltage	H-bridge 1 (V_{dc})	H-bridge 2 (V_{dc})
$+2V_{dc}$	P	P
$+V_{dc}$	P	0
	0	P
0	0	0
$-V_{dc}$	N	0
	0	N
$-2V_{dc}$	N	N

Table 2. Voltage Levels of Nine-level Inverter

Output voltage	H-bridge 1 (V_{dc})	H-bridge 2 ($3V_{dc}$)
$+4V_{dc}$	P	P
$+3V_{dc}$	0	P
$+2V_{dc}$	N	P
$+V_{dc}$	P	0
0	0	0
$-V_{dc}$	N	0
$-2V_{dc}$	P	N
$-3V_{dc}$	0	N
$-4V_{dc}$	N	N

3. SVM in Cascaded H-Bridge Inverter

From the late 1990s, several SVM schemes for multilevel inverters have been introduced. The SVM schemes are based on finding the three nearest space vectors on the space voltage vector hexagon diagram with respect to the reference vector. The mathematical formulation of the SVM methods in the Cartesian coordinate system is quite complex, because the coordinates of the space vectors on the lattice are fractional numbers, which made difficult the space vectors selection. This was until Wei et al. in [18] suggested a coordinate transformation that the reference vector was transformed from the Cartesian coordinate system to the 60° coordinate system. The 60° coordinate system represents one sector on the lattice, and its benefit is that the coordinates for the space vector can be presented by integers. Thus, determination of the space vectors could be accomplished by simple rounding functions and integer calculation [19].

The used SVM method in this paper is similar to [18] which have some changes in switching sequence design. Since the space vector can be presented by integers, this scheme can be used for asymmetrical inverter too. Reference voltage vector location and dwell time calculation for asymmetrical inverter are similar to symmetrical inverter which has equal number of voltage levels, finally the gating signals are made according to the switching sequences to achieve the required voltage level.

The space vector diagram of a three-phase voltage source inverter is a hexagon, consisting of six sectors, which is defined as follows:

$$\vec{V} = V_a e^{j0} + V_b e^{j\frac{2\pi}{3}} + V_c e^{j4\frac{\pi}{3}} \tag{2}$$

where, V_a, V_b and V_c are the phase voltages of the inverter. Here, the operation is explained for the first sector, the same is applicable for other sectors too. Fig. 3 shows space vector diagram for one sector of nine-level inverter, which transformed into 60° coordinates system with α and β axes by following equations:

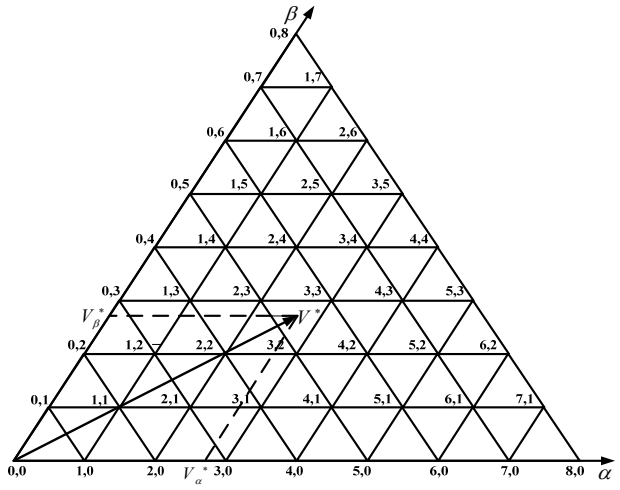

Fig. 3. Space vector diagram of nine-level give space before bracket (sector 1).

$$V_\alpha = \left(\frac{2}{\sqrt{3}}\right)\left(\frac{(n-1)|\vec{V}|}{V_{dc}}\right)\sin\left(\frac{\pi}{3}-\theta\right) \quad (3)$$

$$V_\beta = \left(\frac{2}{\sqrt{3}}\right)\left(\frac{(n-1)|\vec{V}|}{V_{dc}}\right)\sin(\theta) \quad (4)$$

where V_α and V_β are components of V on α and β axes respectively, n is the number of inverter levels, θ is the angle of space vector and V_{dc} is amplitude of each level in n-level inverter.

The SVM method can be categorized in following items:

3.1 Reference voltage vector location

Consider the reference vector $\vec{V}^*$ in Fig. 4. The aim is to identify the triangle where the required reference vector is located and then finding the three nearest space vectors. The space vectors V_E, V_F and V_G can be calculated by following equations:

$$\begin{cases} V_E = (V_{E\alpha}, V_{E\beta}) = (V_{D\alpha}+1, V_{D\beta}) \\ V_F = (V_{F\alpha}, V_{F\beta}) = (V_{D\alpha}, V_{D\beta}+1) \\ V_G = (V_{G\alpha}, V_{G\beta}) = (V_{D\alpha}+1, V_{D\beta}+1) \end{cases} \quad (5)$$

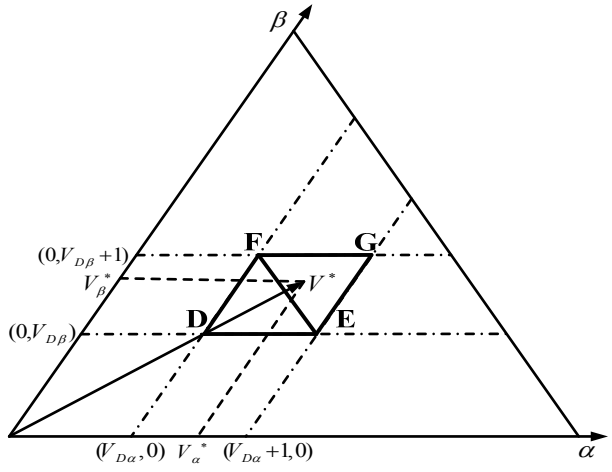

Fig. 4. Decomposition of reference vector.

where, $V_{D\alpha}$ and $V_{D\beta}$ are V_D coordinates which are equal to int(V_α^*) and int(V_β^*), respectively. Int() is a lower rounded integer function. Then following criterion is used to determine which triangular the reference vector lies in.

$$\begin{cases} (V_\alpha^*, V_\beta^*) \le (V_{D\alpha}+V_{D\beta}+1) \rightarrow V^* \in \Delta DEF \\ (V_\alpha^*, V_\beta^*) > (V_{D\alpha}+V_{D\beta}+1) \rightarrow V^* \in \Delta EFG \end{cases} \quad (6)$$

3.2 Dwell time calculation

The following two equations can be established according to the commonly used volt-second balancing principle:

$$\begin{cases} \vec{V}_0 T_0 + \vec{V}_1 T_1 + \vec{V}_2 T_2 = \vec{V}^* T_C \\ T_0 + T_1 + T_2 = T_C \end{cases} \quad (7)$$

where V_0, V_1 and V_2 are vertexes of triangular in space vector diagram, T_0, T_1 and T_2 are dwell times in this vertexes and T_C=1/(2f_s) where f_s is the switching frequency. In accordance with the reference vector lies in triangular *DEF* or *EFG* one of the bellow equations can be used which are obtained from equations (5), (7).

$$V^* \in \Delta DEF \rightarrow \begin{cases} T_E = (V_\alpha^* - V_{D\alpha})T_C \\ T_F = (V_\beta^* - V_{D\beta})T_C \\ T_D = T_C - T_E - T_F \end{cases} \quad (8)$$

$$V^* \in \Delta EFG \rightarrow \begin{cases} T_E = (V_{D\beta} + 1 - V_\beta^*)T_C \\ T_F = (V_{D\alpha} + 1 - V_\alpha^*)T_C \\ T_G = T_C - T_E - T_F \end{cases} \quad (9)$$

3.3 General relationship between space vectors and switching states

Based on equation (2) some switching states are redundancy and create the same space vectors. The numbers of redundant switching states increase with the number of voltage levels. Space vectors in the 60° coordinate system can be generally expressed by (α,β), where, α, β = 1,2,...,2m and m = (n – 1)/2. For space vector (α,β), its switching states [S_a,S_b,S_c] can be determined by:

$$\begin{cases} S_a = \alpha+\beta-m, \alpha+\beta-m+1, \ldots, m \\ S_b = S_a - \alpha \\ S_c = S_a - \alpha - \beta \end{cases} \quad (10)$$

The number of redundancy for each space vector of n-level inverter is equal to: n − (α + β). The number of redundancy is odd or even if (α + β) is even or odd, respectively.

3.4 Switching States Selection and Switching Sequence Design

The number of switching sequences that the first and the last of these must be a redundant space vector increase with the number of redundant states. The aim is designing switching sequence to minimize the total number of switching transitions and fully optimize the harmonic profile of the output voltage. For switching sequence design small and large states are applied for even number redundancy and medium state is applied for odd number redundancy. Small, medium and large states (S_S, S_M, S_L) for

space vector (α, β) calculated by:

$$\begin{cases} S_L = (\frac{\alpha+\beta}{2}+\frac{1}{2}, \frac{\beta-\alpha}{2}+\frac{1}{2}, -\frac{\alpha+\beta}{2}+\frac{1}{2}) \\ S_M = (\frac{\alpha+\beta}{2}, \frac{\beta-\alpha}{2}, -\frac{\alpha+\beta}{2}) \\ S_S = (\frac{\alpha+\beta}{2}-\frac{1}{2}, \frac{\beta-\alpha}{2}-\frac{1}{2}, -\frac{\alpha+\beta}{2}-\frac{1}{2}) \end{cases} \quad (11)$$

E.g. Table 3 can be applied to switching sequence design for Fig. 4. These sequences are for half cycle and for next half the sequences are employed from last to first.

Table 3. Example of Switching Sequence Design

$V_{D\alpha}+V_{D\beta}$	Triangular	Switching Sequences
Odd	DEF	$S_{SD}\rightarrow S_{ME}\rightarrow S_{MF}\rightarrow S_{LD}$
	EFG	$S_{SG}\rightarrow S_{ME}\rightarrow S_{MF}\rightarrow S_{LG}$
Even	DEF	$S_{LE}\rightarrow S_{MD}\rightarrow S_{SF}\rightarrow S_{SE}$ or $S_{LF}\rightarrow S_{LE}\rightarrow S_{MD}\rightarrow S_{SF}$
	EFG	$S_{LE}\rightarrow S_{MG}\rightarrow S_{SF}\rightarrow S_{SE}$ or $S_{LF}\rightarrow S_{LE}\rightarrow S_{MG}\rightarrow S_{SF}$

4. DTC-SVM

Direct Torque Control (DTC) was introduced for induction motors and then generalized for all AC drives [20]. DTC is one of the advanced control schemes for AC drives [21]. It is characterized by simple control algorithm, easy digital implementation and robust operation [10]. The basic principle of this scheme is the direct control of the torque and stator flux by inverter voltage space vector selection. The electromagnetic torque developed by an induction motor can be expressed as:

$$T_e = \frac{3P}{2}\frac{L_m}{\sigma L_s L_r}\lambda_s \lambda_r \sin\sin\theta_{sr} \quad (12)$$

where, θ_{sr} is the angle between the stator flux vector λ_s and rotor flux vector λ_r, P is number of pole pair, L_m, L_s and L_r are magnetizing, stator and rotor inductances, respectively. σ is the total leakage coefficient equal to $1-L_m^2/L_sL_r$. It can be noticed that the torque depends on the stator and rotor fluxes as well as the angle θ_{sr}. The stator flux vector relates the stator voltage vector v_s by:

$$\frac{d\lambda_s(t)}{dt} = v_s(t) - r_s i_s(t) \quad (13)$$

where, i_s and r_s are the stator current and resistance respectively. Maintaining v_s constant over a sample time interval Δt and neglecting the voltage drop on the stator resistance. The integration of equation (13) yields:

$$\Delta\lambda_s(t) = \lambda_s(t) - \lambda_s(t-\Delta t) = \int_{t}^{t-\Delta t} v_s d\tau = v_s \Delta t \quad (14)$$

This shows that the applied voltage determines the change in the stator flux vector [22]. In induction motor the rotor flux due to the large rotor time constant is moving slowly, but the stator flux can be changed immediately. Therefore angle θ_{sr} as well as torque can be changed thanks to the appropriate selection of voltage vector. Fig. 5 shows graphical representation of stator and rotor flux dynamic behaviour.

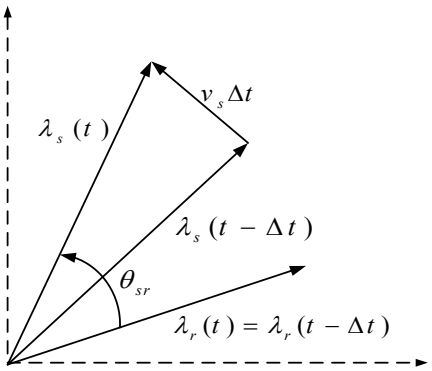

Fig. 5. Influence of v_s over λ_s during a simple interval Δt.

Classical DTC scheme uses hysteresis controllers to select appropriate voltage vector from switching table and generates switching pulses to control the power switches of inverter. This scheme has a simple structure and very good flux and torque dynamic performance. Variable switching frequency, problems during starting and low speed operation, high torque ripples and flux and current distortions are disadvantages of classical DTC that cause of using hysteresis controllers and switching table [11, 23].

Direct flux and torque control with space vector modulation (DTC-SVM) schemes are proposed in order to improve the classical DTC. Basically in DTC-SVM, the controllers calculate the required stator voltage vector and then it is realized by space vector modulation technique. Several methods have been presented for DTC-SVM such as: with PI controllers, with predictive/dead-beat and based on fuzzy logic and/or neural networks. For each of the control structures, different controllers design methods are proposed [11, 24]. DTC-SVM scheme with PI controllers for torque and stator is used here which is shown Fig. 1. Based on the speed error, speed controller calculates reference torque value. The command stator flux is obtained from the reference speed and selected characteristic. Beyond the base speed (field weakening region) the flux is weakened proportional to $1/\omega_r$. These reference values are compared with estimated values which are calculated in the stationary reference frame from terminal measurements by following equations:

$$\lambda_{qs}^{s}(t)=\int_{0}^{t}(v_{qs}^{s}(\tau)-r_{s}i_{qs}^{s}(\tau))d\tau \quad (15)$$

$$\lambda_{ds}^{s}(t)=\int_{0}^{t}(v_{ds}^{s}(\tau)-r_{s}i_{ds}^{s}(\tau))d\tau \quad (16)$$

$$\left|\lambda_{s}^{s}\right|=\sqrt{\lambda_{ds}^{s\,2}+\lambda_{qs}^{s\,2}},\angle\tan^{-1}\tan^{-1}(\frac{\lambda_{qs}^{s}}{\lambda_{ds}^{s}}) \quad (17)$$

$$T_{e}=\frac{3P}{2}(\lambda_{ds}^{s}i_{qs}^{s}-\lambda_{qs}^{s}i_{ds}^{s}) \quad (18)$$

The stator voltage components and electromagnetic torque in stator flux reference frame can be expressed as follows:

$$v_{qs}=r_{s}i_{qs}+\omega_{s}\lambda_{s},\quad v_{ds}=r_{s}i_{ds}+\frac{d\lambda_{s}}{dt} \quad (19)$$

$$T_{e}=\frac{3P}{2}i_{sq}\lambda_{s} \quad (20)$$

With respect to (19), (20) the electromagnetic torque and stator flux can be regulated by v_{qs} and v_{ds}, respectively. Therefore the flux and torque errors across the PI controllers and produce the stator voltage components in stator flux reference frame. These components are DC voltage commands and must be transformed into stationary reference frame in order to use by SVM algorithm which is explained in previous section.

5. Vehicle Dynamic Modeling

The movement behavior of a vehicle along its moving direction is completely determined by all the forces acting on it in this direction [12]. The tractive effort (F_{te}) is the force propelling the vehicle forward to the ground through the driven wheels [25]. This force is available from the propulsion system is partially consumed in overcoming the road load (F_w). The net force, $F_{te} - F_w$, accelerates or decelerates the vehicle [26]. The vehicle acceleration can be written as

$$a=\frac{F_{te}-F_{w}}{k_{m}m} \quad (21)$$

where K_m is the rotational inertia coefficient and m is the vehicle mass.

The road load includes rolling resistance, aerodynamic drag and grading resistance that opposing the vehicle movement.

$$F_{w}=F_{rr}+F_{ad}+F_{gr} \quad (22)$$

The rolling resistance is due to the friction of the vehicle tire on the road.

$$F_{rr}=\mu_{rr}mgcos(\alpha) \quad (23)$$

where g and α are the gravitational acceleration constant and grade angle, respectively. μ_{rr} is the tire rolling resistance coefficient that increases with vehicle velocity and depends on type and pressure of the tire.

The aerodynamic drag is viscous resistance of the vehicle moving through the air. It is mainly function of shape drag and skin friction [12].

$$F_{ad}=0.5\xi C_{ad}A_{f}(v+v_{0})^{2} \quad (24)$$

where ξ, C_{ad} and A_f are air density, aerodynamic drag coefficient and vehicle frontal area, respectively. v and v_0 are vehicle speed and headwind velocity.

The grading resistance appears when a vehicle goes up or down a slope, with positive or negative sign, respectively.

$$F_{gr}=\pm mgsin(\alpha) \quad (25)$$

The power required to drive a vehicle at a speed v is calculated by following equation

$$P_{te}=vF_{te}=v(F_{w}+k_{m}m\frac{dv}{dt}) \quad (26)$$

The mechanical equation (in motor referential) used to describe wheel drive is expressed by

$$T_{m}=T_{L}+B\omega_{m}+J\frac{d\omega_{m}}{dt} \quad (27)$$

where T_m and T_L are the torque of motor and load. B, ω_m and J are the friction factor, the motor mechanical speed and the total inertia, respectively.

The load torque in the motor referential and angular velocity of driven wheel are given by

$$T_{L}=\frac{T_{LWheel}}{i}=\frac{R}{i}F_{w} \quad (28)$$

$$\omega_{Wheel}=\frac{\omega_{m}}{i} \quad (29)$$

where R and i are the wheel radius and transmission ratio, respectively.

The vehicle total inertia in the motor referential is calculated by

$$\begin{cases} J = J_V + J_W \\ J_V = \dfrac{1}{2} m \left(\dfrac{R}{i} \right)^2 (1-\lambda) \end{cases} \quad (30)$$

where J_V and J_W are inertia moment of shaft and wheel, respectively. λ is wheel slip that is usually low and can be neglected, if the adhesion coefficient of the road surface be high [27].

6. FCEV Power Sources Model and Control

6.1 Fuel cell stack model

The fuel cell system consists of Matlab-SimPower Systems based Proton Exchange Membrane Fuel Cell (PEMFC). This generic model is presented in [28] and combines the features of chemical and electrical models which suitable for electrical simulation programs. The fuel cell stack is modeled by a controlled voltage source in series with a constant resistance. The controlled voltage source is function of Tafel slope (A), the exchange current (i_0) and the open circuit voltage (E_{oc}) that will have to be updated based on the input pressures and flow rates, stack temperature and gases compositions [28].

$$E = E_{oc} - NA\ln\left(i_{fc}\right) \quad (31)$$

$$E_{oc} = K_c E_n \quad (32)$$

$$A = \frac{RT}{z\alpha F} \quad (33)$$

$$i_0 = \frac{zFk(P_{H2} + P_{O2})}{Rh} \exp\left(-\frac{\Delta G}{RT}\right) \quad (34)$$

where

i_{fc} = fuel cell current
R = 8.3145 J/(mol K)
N = number of cells
F = 96485 A s/mol
z = number of moving electrons (z = 2)
E_n = Nernst voltage (V)
α = charge transfer coefficient
P_{H2} = partial pressure of hydrogen inside the stack (atm)
P_{O2} = partial pressure of oxygen inside the stack (atm)
k = Boltzmann's constant (1.38×10−23 J/K)
h = Planck's constant (6.626×10−34 J s)
ΔG = activation energy barrier (J)
T = temperature of operation (K)
K_c = voltage constant at nominal condition of operation.

6.2 Battery model

The battery type is Lithium-Ion (Li-Ion) which is based on Matlab-SimPowerSystems library model that is presented in [29]. The battery is modeled using a simple controlled voltage source in series with a constant resistance. The no-load voltage is taken into account with a nonlinear equation based on actual SOC (State-Of-Charge) which has same characteristics for the charge and the discharge cycle [29].

The no-load voltage (E) and the battery voltage (V_{batt}) are calculated by

$$E = E_0 - K\frac{Q}{Q - it} + \text{Aexp}(-B.it) \quad (35)$$

$$V_{batt} = E - R.i \quad (36)$$

where

E_0 = battery constant voltage (V)
K = polarization voltage (V)
Q = battery capacity (Ah)
it = actual battery charge (Ah)
A = exponential zone amplitude (V)
B = exponential zone time constant inverse $(\text{Ah})^{-1}$
R = internal resistance (Ω)
i = battery current (A)

6.3 Power control

6.3.1 Energy management unit

The motor reference power and torque are calculated based on the reference speed and vehicle dynamic. The reference current of fuel cell is determined by the reference power and P-I curve of fuel cell and is sent to DC/DC converter controller. The energy management unit controls the reference power of fuel cell based on the required power of fuel cell and battery recharge power. In this paper one fuel cell and one battery are used as power source for each cell of cascaded H-bridge inverter. The required power of motor is divided among all cells based on their voltages. It should be considered that the battery is used to assist the fuel cell stack.

6.3.2 DC/DC converter

The boost DC/DC converter step up the fuel cell stacks voltage to match that of the DC bus of H-bridge cells. The fuel cell current follows the fuel cell reference current by a current regulator that it uses a PI controller. The duty cycle is derived from the controller that it controls the output power of converter.

7. Simulation Results

To investigate the performance of cascaded H-bridge multilevel inverter in considered motor drive and The SVM method used with multilevel inverter, Matlab-Simulink based five-level and nine-level inverters are employed in

both classic DTC and DTC-SVM based 3hp FCEV induction motor. Two types of PEM fuel cell stack (700W-20V and 300W-12V) are used in simulations. The parameters of induction motor, fuel cell stacks, battery and vehicle dynamic are given in appendix.

The European ECE-15 driving cycle is used as a test cycle, which is useful for testing the performance of small vehicles. A driving cycle is a series of data points representing the vehicle speed versus time. ECE-15 driving cycle is shown in Fig. 6, which has a top speed of 50 km/h. The energy management units divide reference power among cells based on their DC link voltages. Figs. 7, 8 show the rotor speed and the power demanded to drive the vehicle that is calculated by vehicle dynamic.

Fig. 9 shows stator line voltage waveforms for five-level and nine-level cascaded H-bridge inverters. The SVM switching frequency and sampling time are 5 kHz and 20 µs, respectively. As presented in Fig. 9, the stator line voltage using both DTC and DTC-SVM approaches is closed to sinusoidal. Although the SVM modulator synthesizes AC voltage with better approximation of desired sinusoidal waveform. Furthermore Output voltage of asymmetrical inverter in both techniques has more levels and higher quality, consequently the need for output filter can be declined.

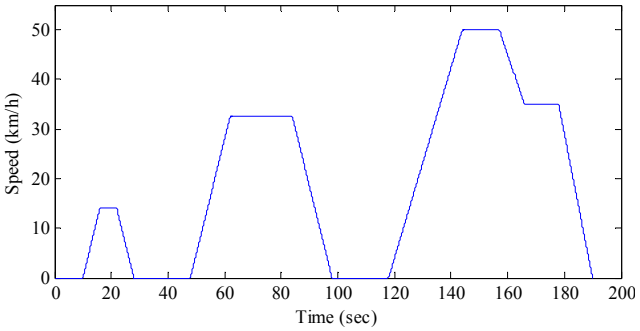

Fig. 6. ECE−15 driving cycle

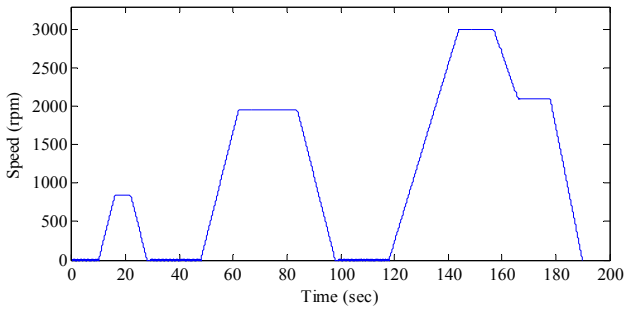

Fig. 7. The speed of rotor

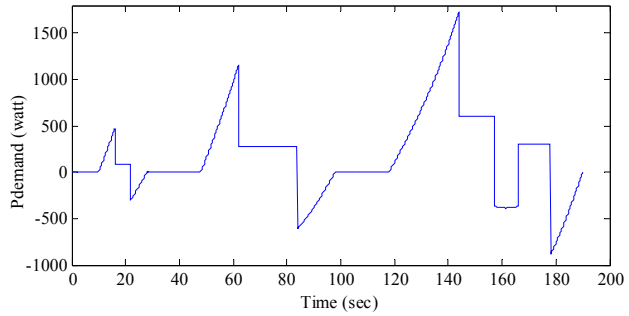

Fig. 8. The power demanded to drive the vehicle.

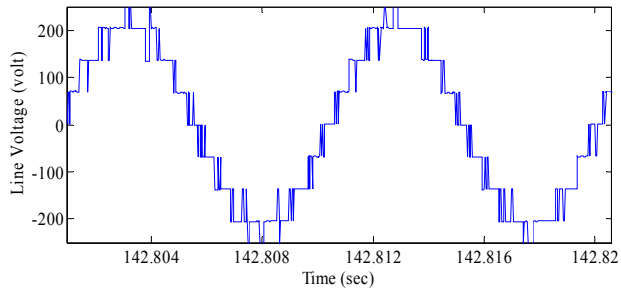

(a)

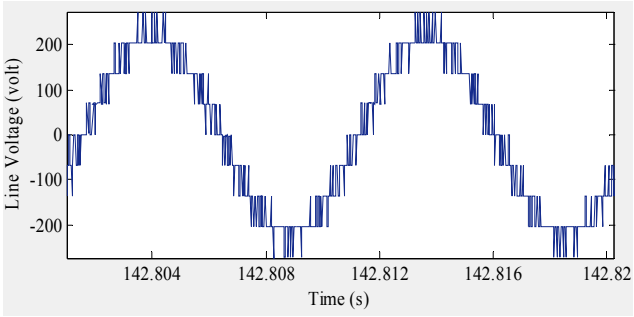

(b)

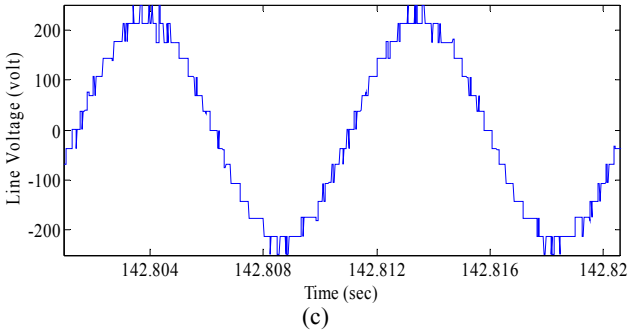

(c)

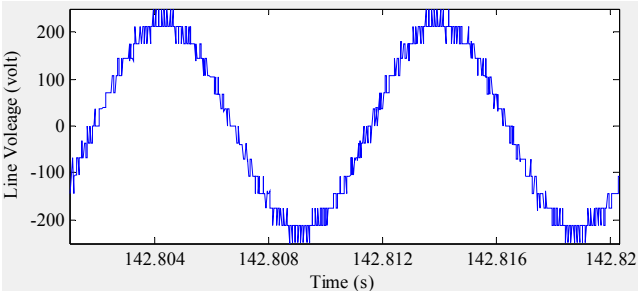

(d)

Fig. 9. Line voltage waveforms: (a) five-level inverter using DTC; (b) five-level inverter using DTC-SVM; (c) nine-level inverter using DTC; (d) nine-level inverter using DTC-SVM.

Fig. 10 shows the induction motor current waveforms. They appear completely sinusoidal, furthermore with using DTC-SVM technique and increasing the number of voltage levels, distortions and ripples decrease in current.

Fig. 11 presents torque dynamic responses of five-level and nine-level inverters. It's clear that the DTC-SVM improves classic DTC torque responses and reduces torque ripples. Also an increase in the number of voltage levels has the same consequence in improvement of the torque quality.

The stator flux waveforms are shown in Fig. 12. The stator flux reference is 0.3Wb that decreases proportional to $1/\omega_r$ in field weakening region. It can be observed that both classic DTC and DTC-SVM techniques have considerably good performance. Of course using the asymmetrical inverter with more voltage levels reduces flux ripples. It's confirming the high dynamic performance

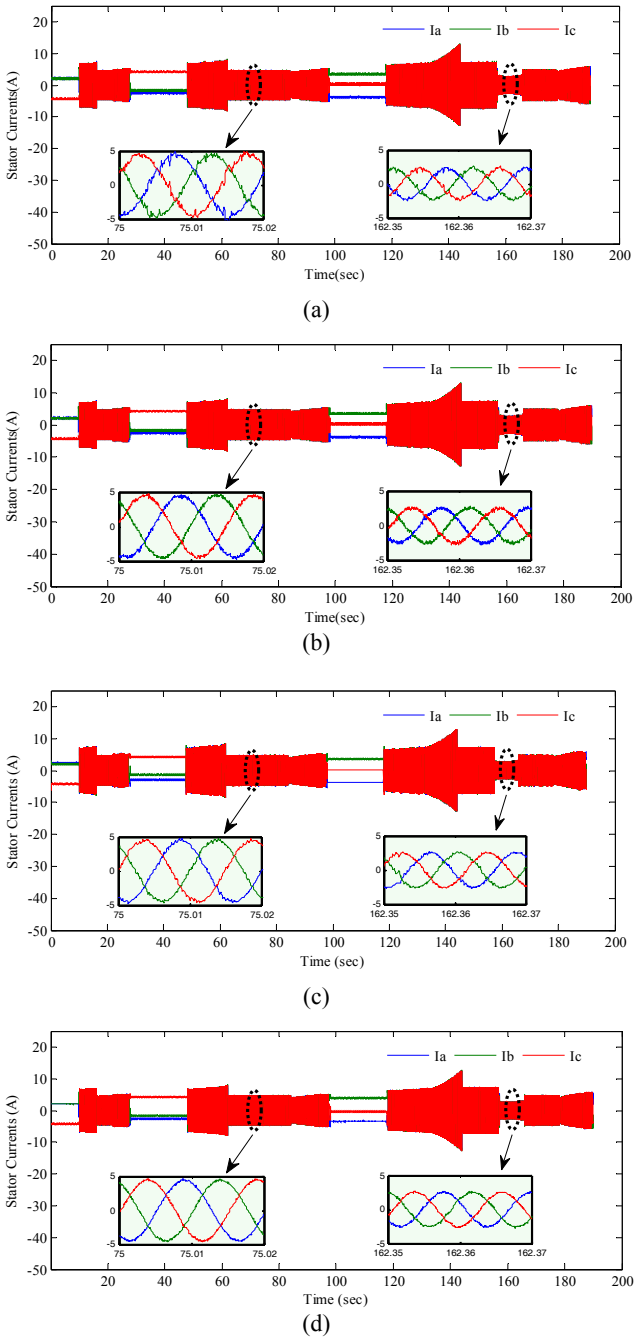

Fig. 10. Stator current waveforms: (a) five-level inverter using DTC; (b) five-level inverter using DTC-SVM; (c) nine-level inverter using DTC; (d) nine-level inverter using DTC-SVM.

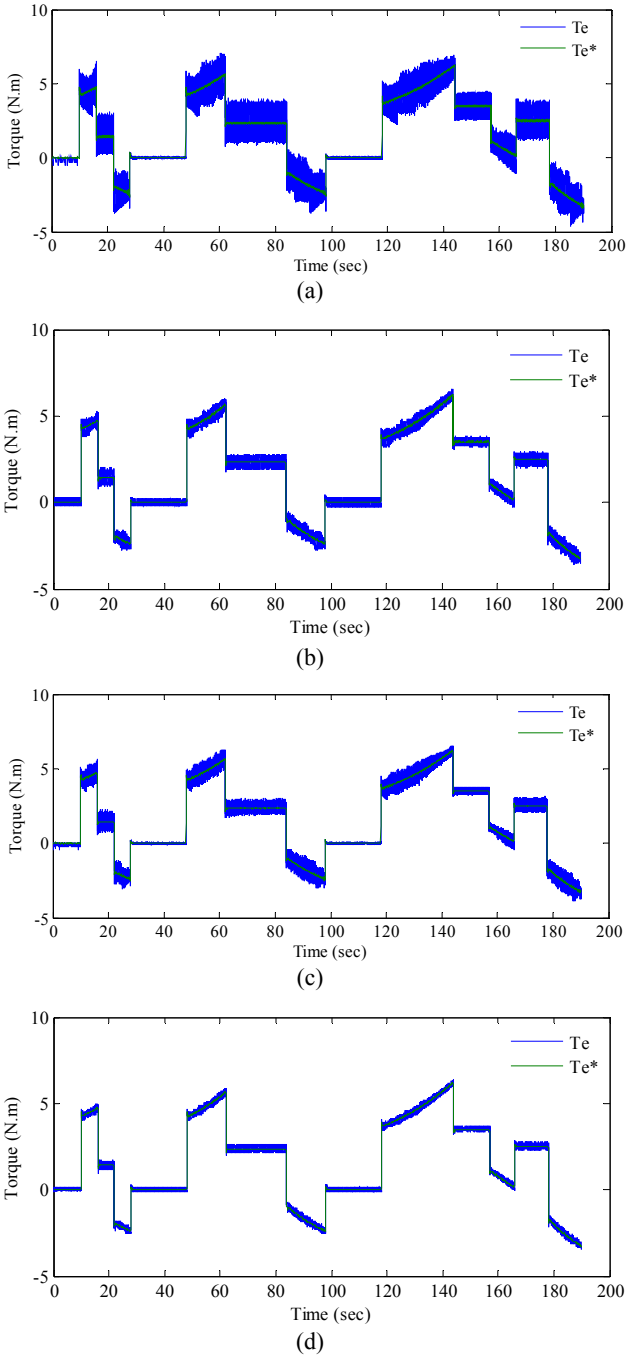

Fig. 11. Torque dynamic responses: (a) five-level inverter using DTC; (b) five-level inverter using DTC-SVM; (c) nine-level inverter using DTC; (d) nine-level inverter using DTC-SVM.

of the perceived drive.

As it is obvious in the results, the drive and DC/DC converter controllers provide good regulation for torque, flux, speed and power. It is noticeable that the asymmetrical arrangement results the better responses than symmetrical inverter by using equal number of power switches.

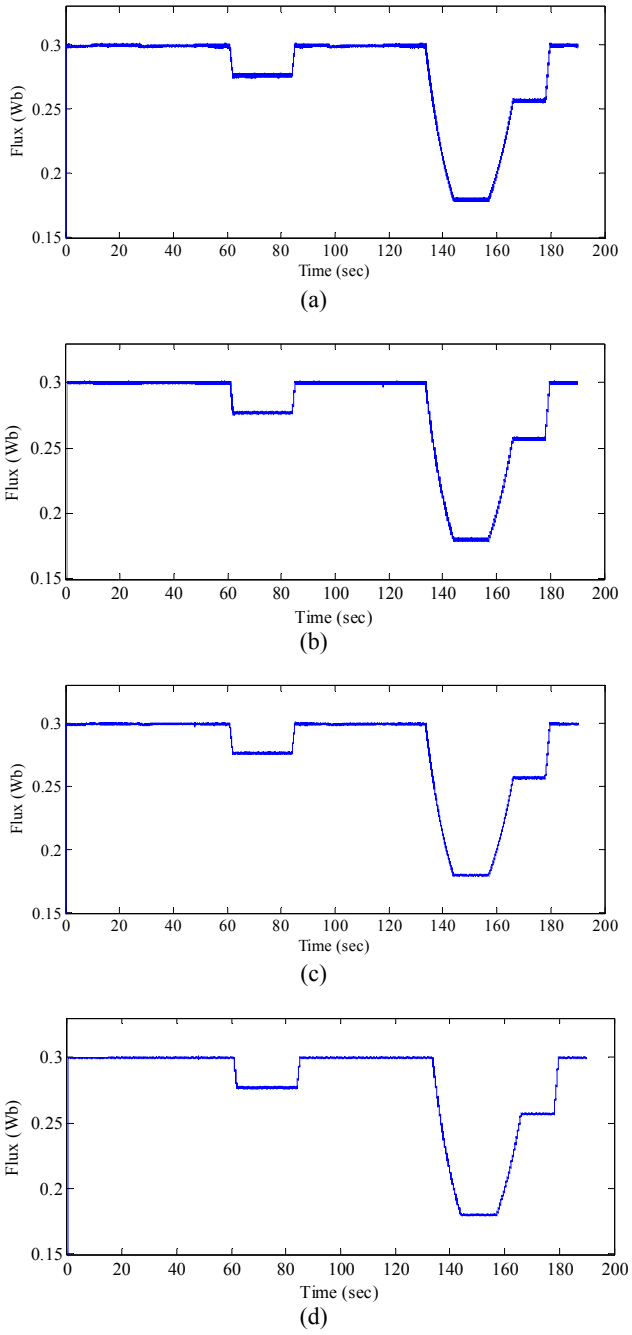

Fig. 12. Stator flux waveforms: (a) five-level inverter using DTC; (b) five-level inverter using DTC-SVM; (c) nine-level inverter using DTC; (d) nine-level inverter using DTC-SVM.

8. Conclusion

Cascaded H-bridge multilevel inverter for 3hp FCEV DTC-SVM based induction motor drive has been provided in this paper. To illustrate the performance of SVM technique used with multilevel inverter, simulation has been carried out using classic DTC scheme too. Five-level and nine-level multilevel inverters have been used in simulations. A fuel cell and battery has been employed as a power source of each H-bridge cell. Consequently the performance of the induction motor drive has increased. Contribution of multilevel inverter in motor drive for FCEV application led to get near sinusoidal stator voltage, very low ripples in current, less distortion and good regulations of torque and stator flux. Simulation results demonstrated the superiority of DTC-SVM method over classic DTC and the great performance of cascaded H-bridge multilevel inverter in DTC-SVM based induction motor drive for FCEV application. Furthermore with increase the number of voltage levels in asymmetrical inverter the drive performance has been increased by equal number of power switches.

Appendix

The Parameters of Induction Motor

$3\ hp, 60\ Hz, 220\ \text{V}, 1710\ \text{rpm}, \text{P} = 2$

$R_s = 0.435\,\Omega, R_r = 0.816\,\Omega$

$L_s = 2\ mH, L_r = 2\ mH, L_m = 69.3\ mH$

$J = 0.089\ kg.m^2, \beta = 0.005\ N.m.s$

Vehicle Parameters

m = 140 kg, A_f = 0.8 m^2, R = 0.23 m,
μ_{rr} = 0.015, C_{ad} = 0.25, g = 9.81 m/s^2,
k_m = 1.08, ξ = 1.202 kg/m^3, i = 5.2025

Battery Parameters

Parameters	Li-Ion (97.5V,1Ah)	Li-Ion (32.5V,1Ah)
Initial SOC (%)	40.32	40.32
Fully charged voltage(V)	113.4887	37.8269
Internal resistance(Ω)	0.975	0.325
Exponential zone [voltage(V),capacity(Ah)]	[105.31,0.0491]	[35.11,0.0491]

Fuel Cell Stacks Parameters

Parameters	PEMFC 700W	PEMFC 300W
E_{oc} (V)	28.8	17.5
[I_{nom}(A), V_{nom}(V)]	[35,20]	[25,12]
[I_{max}(A), V_{max}(V)]	[51.5152,16.5]	[40,10]
N	30	20
T (°C)	55	55
η (%)	46	46
[P_{fuel}(bar), P_{air}(bar)]	[1.5,1]	[1.5,1]

References

[1] J. Rodríguez, J. Lai, and F. Peng, "Multilevel converters: a survey of topologies, controls and applications," *IEEE Trans. Ind. Electron*., Vol. 49, No. 4, pp. 724-738, Aug. 2002.

[2] L. M. Tolbert, F. Z. Peng, and T. G. Habetler, "Multilevel converters for large electric drives," *IEEE Trans. Ind. Appl.*, Vol. 35, No. 1, pp. 36-44, Jan./Feb. 1999.

[3] J. S. Lai and F. Z. Peng, "Multilevel converters – A new breed of power converters," *IEEE Trans. Ind. Appl.*, Vol.32, No.3, pp. 509-517, May/Jun. 1996.

[4] Z. Du, L. M. Tolbert, B. Ozpineci, J. N. Chiasson, "Fundamental frequency switching strategies of a seven-level hybrid cascaded H-bridge multilevel inverter," *IEEE Trans. Power Electron.,* Vol. 24, No. 1, pp. 25-33, Jan. 2009.

[5] R. Salehi, B. Vahidi, N. Farokhnia and M. Abedi, "Harmonic elimination and optimization of stepped voltage of multilevel inverter by bacterial foraging algorithm", *Journal of Electrical Engineering & Technology.* Vol. 5, No. 4, pp. 545~551, 2010.

[6] F. Khoucha, S. M. Lagoun, K. Marouani, A. Kheloui, and M. E. H. Benbouzid, "Hybrid cascaded H-bridge multilevel-inverter induction-motor-drive direct torque control for automotive applications," *IEEE Trans. Ind. Electron.,* Vol. 57, No. 3, pp. 892-899, Mar. 2010.

[7] Y. S. Lai and F. S. Shyu, "Topology for hybrid multilevel inverter," *Proc. Inst. Elect. Eng. —Electr. Power Appl.*, Vol. 149, No. 6, pp. 449-458, Nov. 2002.

[8] M. Veenstra and A. Rufer, "Control of a hybrid asymmetric multilevel inverter for competitive medium-voltage industrial drives," *IEEE Trans. Ind. Appl.*, Vol. 41, No. 2, pp. 655-664, Mar./Apr. 2005.

[9] C. Rech and J. R. Pinheiro, "Hybrid multilevel converters: Unified analysis and design considerations," *IEEE Trans. Ind. Electron.*, Vol. 54, No. 2, pp. 1092-1104, Apr. 2007.

[10] D. Casadei, F. Profumo, A. Tani, "FOC and DTC: two viable schemes for induction motors torque control", *IEEE Trans. Power Electron.* Vol.17, No. 5, pp. 779-787. Sep. 2002.

[11] M. Żelechowski, Space vector modulated – direct torque controlled (DTC – SVM) inverter – fed induction motor drive, PhD Thesis, Warsaw University of Technology, 2005.

[12] M. Ehsani, Y. Gao, and A. Emadi, *Modern Electric, HybridElectric, and Fuel Cell Vehicles: Fundamentals, Theory, and Design*. Boca Raton, FL: CRC, 2010.

[13] L. M. Tolbert, F. Z. Peng, and T. G. Habetler, "Multilevel inverters for electric vehicle applications," in *Proc. IEEE Workshop Power Electron Transportation,* Dearborn, MI. pp. 79-84. Oct. 22-23, 1998.

[14] L. M. Tolbert, F. Z. Peng, T. Cunnyngham, and J. Chiasson, "Charge balance control schemes for cascade multilevel converter in hybrid electric vehicles," *IEEE Trans. Ind. Electron,* Vol. 49, No. 5, pp. 1058-1064, Oct. 2002.

[15] F. Khoucha, S. M. Lagoun, K. Marouani, A. Kheloui, and M. E. H. Benbouzid, "A comparison of symmetrical and asymmetrical three-phase H-bridge multilevel inverter for DTC induction motor drives," *IEEE Trans. Energy Conversion,* Vol. 26, No. 1, pp. 64-72, Mar. 2011.

[16] P. W. Hammond, "A new approach to enhance power quality for medium voltage ac drives", *IEEE Trans. Ind. Appl.* Vol. 33, No. 1, pp. 202-208, 1997.

[17] Bin Wu, High-power converters and ac drives, Toronto, 2006.

[18] Wei, S., Wu, B., Li, F., and Liu, C, "A general space vector PWM control algorithm for multilevel inverters", *APEC '03*, Vol. 1, pp. 562-568. 2003.

[19] Naumanen. V, Multilevel converter modulation: Implementation and analysis, PhD Thesis, Finland University of Technology Lappeenranta, 2010.

[20] Ion. Boldea, Control in power electronics, Romania University Politehnica, Timisoara.

[21] J. N. Nash, "Direct torque control, induction motor vector control without an encoder, ", *IEEE Trans. Ind. Appl.,* Vol. 33, No. 2, pp. 333-341, 1997.

[22] J. Rodriguez, J. Pontt, S. Kouro, and P. Correa, "Direct torque control with imposed switching frequency in an 11-level cascaded inverter," *IEEE Trans. Ind. Electron.*, Vol. 51, No. 4, pp. 827-833, Aug. 2008.

[23] Z. Boulghasoul, A. Elbacha and E. Elwarraki, "Intelligent control for torque ripple minimization in combined vector and direct controls for high performance of IM drive", *Journal of Electrical Engineering & Technology.* Vol. 7, No. 4, pp. 546~ 557, 2012.

[24] G. S. Buja, M. P. Kazmierkowski, "Direct torque control of pwm inverter-fed ac motors—A survey," *IEEE Trans. Ind. Electron.*, Vol. 51, No. 4, Aug. 2004.

[25] J. Larminie, J. Lowry, *Electric Vehicle Technology Explained.* West Sussex PO19 8SQ, England, 2003.

[26] M. Ehsani *et al.*, "Propulsion system design of electric and hybrid vehicle," *IEEE Trans. Ind. Electron.*, Vol. 45, No. 1, pp. 19-27, Feb. 1997.

[27] A. Haddoun *et al.*, "A loss-minimization DTC scheme for EV induction motors," *IEEE Trans. Veh. Technol.*, Vol. 56, No. 1, pp. 81-88, Jan. 2007.

[28] S. Njoya M, O. Tremblay, and L.-A. Dessaint, "A generic fuel cell model for the simulation of fuel cell vehicles," *Vehicle Power and Propulsion Conference*, *VPPC,* pp. 1722-1729, Sep. 2009.

[29] O. Tremblay, L.-A. Dessaint, A.-I. Dekkiche, "A generic battery model for the dynamic simulation of hybrid electric vehicles," *Vehicle Power and Propulsion Conference*, *VPPC,* pp. 284-289, Sep. 2007.

Javad Gholinezhad was born in Gorgan, Iran, in 1986. He received his B.Sc. degree in Electrical Engineering from Babol University of Technology, Babol, Iran, in 2009, and his M.S. degree in Electrical Engineering from University of Zanjan, Zanjan, Iran, in 2012. His research interests are modeling and control of power electronic converters, electrical drives, power system stability and protection.

Reza Noroozian was born in Iran. He is an assistant professor with the department of Power Engineering, University of Zanjan, Iran. He received his B.Sc. from Tabriz University, Tabriz, Iran, in 2000. He received his M.Sc. and also Ph.D. degrees in electrical engineering from Amirkabir University of Technology (AUT), Iran, in 2003 and 2008, respectively. His areas of interest include: Power Electronic, Power System, Power Quality, Integration and Control of Renewable Generation Units, Custom Power, Micro-grid Operation, Distributed Generation Modeling, Operation and Interface Control. Dr Noroozian is a member of the Institute of Electrical and Electronics Engineers (IEEE).